

Research Article

Development of a Novel Switched-Mode 2.45 GHz Microwave Multiapplicator Ablation System

Guido Biffi Gentili,¹ Cosimo Ignesti,² and Vasco Tesi³

¹ Department of Information Engineering, University of Florence, Via di S. Marta 3, 50139 Florence, Italy

² Biomedical Srl, Via G.B. Lulli 43, 50144 Florence, Italy

³ WaveComm S.r.l., Loc. Belvedere, Ingresso 2, 53034 Colle Val d'Elsa, Siena, Italy

Correspondence should be addressed to Cosimo Ignesti; cosimo.ignesti@gmail.com

Received 29 May 2014; Revised 7 August 2014; Accepted 25 August 2014; Published 23 September 2014

Academic Editor: Gian Luigi Gragnani

Copyright © 2014 Guido Biffi Gentili et al. This is an open access article distributed under the Creative Commons Attribution License, which permits unrestricted use, distribution, and reproduction in any medium, provided the original work is properly cited.

The development of a novel switched-mode 2.45 GHz microwave (MW) multiapplicator system intended for laparoscopic and open surgical thermoablative treatments is presented. The system differs from the other synchronous and asynchronous commercially available equipments because it employs a fast sequential switching (FSS) technique for feeding an array of up to four high efficiency MW applicators. FSS technology, if properly engineered, allows improving system compactness, modularity, overall efficiency, and operational flexibility. Full-wave electromagnetic (EM) and thermal (TH) simulations have been made to confirm the expected performances of the FSS technology. Here we provide an overview of technical details and early *ex-vivo* experiments carried out with a full functional β -prototype of the system.

1. Introduction

In cancer treatment, open surgery and chemotherapy are still the physicians' first choices. The gold standard treatment for most of the tumors in the liver, lung, and kidney is surgical resection. However, up to 80% of liver cancer patients and 50% of lung cancer patients are refractory to surgery due to multifocal disease, poor baseline health, or comorbidities such as cirrhosis and emphysema [1, 2]: for some patients, removal of tumors with open surgery is not possible or involves a too high risk due to the poor condition of the patient himself. Therefore their success rate largely depends on the type of malignancy treated and on the progress of the disease.

Minimally invasive surgery or percutaneous interventions may in these cases be adequate to increase safety, reduce trauma, and shorten operative time [3–5].

Microwave ablation (MWA) is a relatively new technology in continuous development because it offers some advantages when compared to the radiofrequency ablation (RFA) [6–8], the technology which currently represents the prevailing clinical focal therapy. MWA can generate higher

temperatures in less time since tissue charring does not hinder the radiation of MW fields and it is less susceptible to the *heat-sink effect* of peritumoral vessels [9]. For these reasons, MWA and their minimally invasive approach have fertile ground for innovation through future systems and technological developments. Clinical MWA equipment operate at 915 MHz or 2.45 GHz since these bands, which are allowed for medical use and relatively high-power devices, are readily available providing a balance between localized heating and sufficient energy penetration to treat most focal tumors [10].

The power that the coaxial structure of a microwave applicator can safely handle is proportional to its external diameter; therefore very small diameter applicators can handle proportionally smaller powers. This physical limit can be overcome by cooling the applicator shaft or by combining more than one antenna into an array of applicators in order to increase the coagulation volume [11, 12]. However, due to the high losses of the internal coaxial feeding line, a small diameter shaft cooled antenna intrinsically suffers of low radiating efficiency that rapidly falls with the decreasing of its external diameter.

A single applicator appears fundamentally unable to uniformly and efficiently heat a large volume of tissue because the emitted radiation is subjected to a very strong attenuation, due to the intrinsic high propagation losses of the biological tissue. Recent researches [10, 13] show a fundamental advantage in using multiple antennas: power distribution in a multiple-probe system is more effective, even compared to that of a single antenna providing the same amount of energy. Heating produced simultaneously by multiple nearby synchronous (coherent) or asynchronous (incoherent) arrays of radiating sources can create larger ablation areas than what we might expect from a single applicator radiating the same amount of energy, by means of the effect called *thermal synergy* [14]. This ability to perform multiple ablation simultaneously may allow the treatment of large tumors with concurrent overlapping thermal lesions or the ablation of several anatomically separate tumor lesions at once [11].

The median tumor diameter currently being targeted by thermal ablation is approximately 25 mm. Therefore, a 35–40 mm ablation zone is recommended to treat an average tumor with an appropriate 5–10 mm radial margin, aiming at a lower probability of local tumor progression [15, 16].

Furthermore properly assembled linear or conformal arrays of applicators can be used as surgical resection devices to reduce blood losses and to assist in coagulation of liver tissue during intraoperative and laparoscopic surgical procedures.

Multiprobe ablations reduce the need to repeat treatments, decrease inadequate treatments of larger tumors, and increase the speed of the therapy, thereby decreasing the complication rate.

The purpose of this paper is to present the development of a novel 2.45 GHz multiprobe modular thermoablation system conceived to reduce system complexity and cost while maintaining a very high energetic efficiency.

The simplest way to implement a MWA N -needle ablative system consists in the simultaneous use of N power generators, where each generator independently feeds an applicator of the array but does not communicate with the others.

This obvious asynchronous solution is certainly not optimal from the engineering point of view because solid-state MW power generators are very expensive and a separate control unit ought to be used because independent control of each generator is impractical in the clinical environment.

Alternatively N microwave power amplifiers (MPA) fed in parallel by a common low-power MW source could be employed, leading to a synchronous or coherent solution that allows phase control of the array. In principle this solution should offer better energy focalization inside the tumor by taking advantage of near-field array optimal phasing. In practice, however, the heat diffusion in the perfused tissue smoothes the behavior of the temperature distribution inside the treated volume (See Appendix A), thus drastically reducing the advantages of the coherent feeding.

The use of multiple generators/amplifiers can be avoided by employing a single generator and a passive power splitter as shown in Figure 1.

This straightforward solution allows reducing system complexity and costs but suffers of poor flexibility because

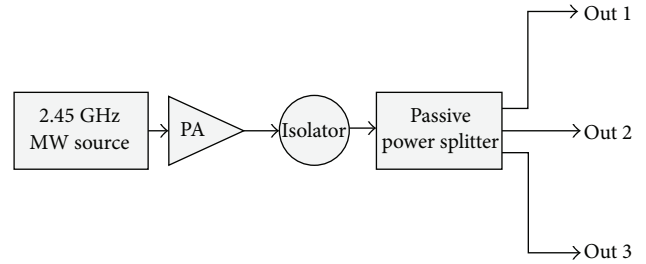


FIGURE 1: Block diagram of a single generator multioutputs MWA system.

the total available power P_{tot} at the generator output port is equally split among N ports; therefore when only a single applicator is used, the maximum allowable power is P_{tot}/N , unless the splitter is removed.

To overcome this limitation and to increase system flexibility and usability, the power distribution among N applicators can be done using a switched-mode approach [17] where the N applicators of the array are fed sequentially in time using a very fast solid-state high power switch, as early proposed in [18].

This approach leads to a simple and highly flexible solution called fast sequential switching (FSS), where the switching frequency must be kept high enough to prevent localized temperature drop during the applicator's off-time. By adjusting the duty-cycle of the signal that drives the switch, "on-the-fly" corrections or adaptive control of the power distribution among the N applicators can be done without any energy loss.

In Section 2 we outline the system concept and in Section 3 we describe the engineering development of the new equipment. Section 4 concerns the critical aspects of system safety and risk management; finally the conclusions are presented in Section 5.

Two appendices are included to assist the reader in recognizing the potentialities of the new multiapplicator system. Appendix A is devoted to the numerical modeling of a single and a dual applicator immersed in a muscle phantom; Appendix B reports some significant *ex vivo* experiments in swine liver and loin.

2. System Concept

The system has been conceived to evolve from the usual single applicator system to the new four-applicator FSS technology with the following objectives:

- (i) addressing the perceived deficiencies in first-generation systems;
- (ii) treating larger tumors, improving ablative margins and decreasing treatment time;
- (iii) improving flexibility, usability, and procedural safety.

The system concept is based on the fact that the thermal time constant τ of a biological tissue is relatively high (in the order of seconds); thus if MW power is applied in

a periodic pulsed mode with a short pulse period, the tissue temperature tends to be related to the average applied power. Therefore we can conceive a switched-mode regulator that uses a continuous wave (CW) source with the output power P that is periodically switched ON/OFF to a load (tissue to be ablated) with period T , thus transferring to it a controlled fraction of the power P . The lower useful limit of T is given by the commutation time of the switch while the upper limit is given by the ratio T/τ that should be <1 . It was experimentally found that using a period T between 0.5 and 2 seconds the switched-mode system is practically equivalent to an ideal asynchronous system.

During a therapy session the power P is generally held constant and equal to the total power P_t that the physician wants to dispense to the tumor through a set of applicators:

$$P = P_t = \sum P_k \quad \text{with } k = 1 \dots 4. \quad (1)$$

The power distribution can be easily obtained using four very fast switches; the ON time of the k th switch is given by

$$T_k = \frac{T \cdot P_k}{P_t}. \quad (2)$$

When a single applicator is employed only the corresponding switch is always ON, while the others are OFF.

3. System Development

We believe that cross-collaboration is essential for the success of our project. Such partnership is also necessary to produce novel and commercially viable technologies. Furthermore, consistent inputs from a team of clinical experts are crucial to ensure that the developed technology remains clinically relevant and, therefore, can have the greatest positive impact on the rapid diffusion of minimally invasive focal treatments at MW frequencies.

With this in mind, a fully engineered prototype of the novel switched-mode system, called thermal ablation multiprobe microwave system (TAMMS), has been developed by a small multidisciplinary team at the University of Florence, in the framework of a collaborative academic-industry agreement with two private companies: Biomedical Srl, Florence (<http://www.biomedical-srl.com/>), that provided financial support and laboratory facilities, and WaveComm Srl, Siena (<http://www.wavecomm.it/>), that provided qualified engineering support.

As shown in Figure 2, TAMMS consists of the following main blocks:

- (i) a single 100 W high efficiency solid-state MW power generator working at 2.45 GHz;
- (ii) an FSS microwave switching unit (MSU), which operates as a programmable “active” power splitter. This unit has four IN/OUT ports that can be automatically configured as output power ports (100 W maximum) or temperature sensing input ports;
- (iii) a controller that regulates the MW generator power output and produces the time sequence that commands the single pole 4 throw (SP4T) switch of the FSS unit;

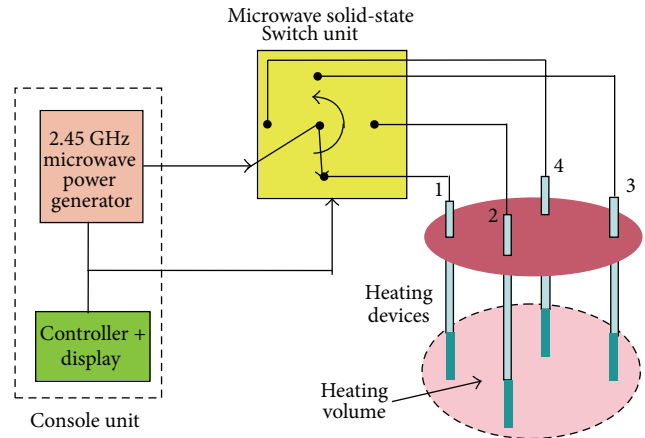


FIGURE 2: Block diagram of the four-applicator TAMMS system employing FSS technology.



FIGURE 3: TAMMS 3D rendering.

- (iv) a rugged power delivery device (interstitial applicator) in 18, 17, and 14 gauge formats preferred for percutaneous procedures and 11 gauge format for surgical applications. For high power treatments all the devices can be cryogenically cooled using CO_2 .

In order to optimize the overall efficiency, the system has been designed with a two-stage power distribution concept: the first stage utilizes a large low loss coaxial cable that connects the MW power generator to the MSU, while the second stage comprises smaller more flexible cables connecting the MSU outputs to the corresponding power delivery devices.

Figure 3 shows the 3D rendering of the new system that evidences its compactness and the attention paid to the fundamental aspects of ergonomics, usability, and safety (industrial design made by Un-Real Studio, Florence, Italy—<http://www.un-real.it/>).

A robust and balanced mechanical arm with a double through-joint allows positioning the MSU nearby the patient

to reduce the length of the cables that connect the unit to the set of interstitial applicators. Alternatively the MSU can be connected to the procedure bed in order to be fixed relative to patient. It is worth noting that if the MSU is omitted the system reduces to a conventional single applicator thermoablator with 100 W maximum CW power output.

3.1. Console Unit. The console unit contains four main blocks: a solid-state MW generator, a switching AC/DC power supply, a digital controller, and a touch screen display.

The MW generator is capable of delivering a power output in excess of 100 W. The last-generation solid-state gallium nitride on silicon carbide (GaN-on-SiC) class AB high power amplifier (HPA), having 50% power added efficiency (PAE) at 100 W power output, can withstand 10 : 1 VSWR without damage. Furthermore automatic shut-off is provided for higher mismatching levels. The generator integrates multiple protection methodologies, including a forward power detector, a reflection power detector, and an embedded microcontroller to control alarm features. A forced air cooling system maintains the internal temperature of the whole generator below 75°C.

The 400 W medical grade AC/DC switching power supply has power efficiency in excess of 90% and automatic overload shutoff to further protect the MW generator.

The digital control unit performs core safety critical tasks by a board based on a powerful mixed signal microcontroller while the human-machine interface (HMI) is implemented by a high level program running on a single board computer (SBC) under Linux operating system.

The color touchscreen display has 800 × 480 pixel and the capability of showing multiple interactive screenshots dedicated to set the treatment parameters, monitor their evolution, and display devices status in real time.

The console has 35 × 32 × 15 cm overall dimensions and weighs less than 8 Kg to be possibly hand carried and/or connected to a classical instrument stand.

3.2. Microwave Switching Unit. The MSU represents a well-balanced tradeoff between system flexibility in terms of ablation volume/shape and complexity/compactness/cost of the switching MW circuitry.

The unit utilizes a matrix of high power PIN diodes as switching elements in a SP4T configuration. The design goal was to maintain the internal insertion losses <0.5 dB with resulting high system efficiency and low heat dissipation. An aluminum case provides both heat dissipation by natural convection and EM shielding. Table 1 resumes its main characteristics.

Figure 4 illustrates the realized MSU in microstrip planar technology with the cover removed.

Figure 5 depicts the unit operation in the time domain when the generator available power is equally subdivided among four applicators; in this case the driving sequence duty-cycle $D_t = T_{on}/T_{off}$ is 0.25 for all applicators.

The MSU receives commands from the console via a serial bus interface and an embedded controller locally generates the appropriate PIN diodes driving time sequences. It is

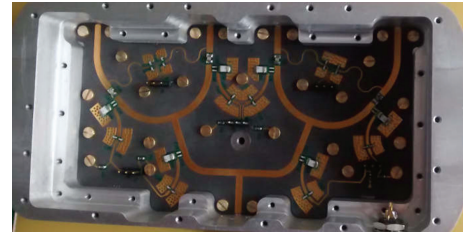


FIGURE 4: Microwave switching unit, inside view.

TABLE 1: Characteristics of the high power SP4T switching unit.

Parameter	Typical	Limit
Frequency (GHz)	2.45	ISM band
VSWR	1.13 : 1	<1.4 : 1
Insertion loss (dB)	0.4	<0.6
Power handling capability (W)	100	<150
Switching time (μ S)	200	500

worth noting that anyway the total delivered power did not exceed 100 W that corresponds to the maximum allowable generator output power; this constraint is automatically verified by the console controller.

3.3. Power Delivery Device. The power delivery device has a mechanically simple and rugged coaxial structure outlined in Figure 6 that consists of a dielectrically loaded monopole with a capacitive cap [19–21] fed by a coaxial line.

The device derives from the one described in [18], where the radiating element was a simple linear monopole. A needle shaped cap loading has been introduced to allow easy insertion inside the tissue, reduce the monopole length, and increase tip robustness while maintaining good input matching and radiating performances.

The intrinsically unbalanced design allows returning current flow on the outer conductor influencing impedance matching and producing the so-called “tail comet effect” on the radiated fields that can be reduced by inserting a “cancelling slot” [22]. An equivalent effect could be obtained using a $\lambda/4$ choke as suggested in [23]; this solution is, however, more mechanically complex and does not allow reducing shaft diameter below the 16 G dimension.

A comparison between slotted and unslotted applicators is presented in Appendix A.

It is worth noting that the applicator’s structure (patent pending) is easily scalable and that the very thin commercial semirigid coax cable usually employed for feeding the radiating section of the applicator is avoided, thus simplifying design and reducing insertion losses. Stainless steel inner and outer conductors of the shaft assure high rigidity and robustness of the needle structure; in particular the radiating monopole is simply obtained by lengthening the inner conductor of the shaft, thus assuring very high breaking strength due to the absence of any mechanical junction. The whole device with its handle is shown in Figure 7; in order to reduce the adhesion of charred tissue during the thermoablative

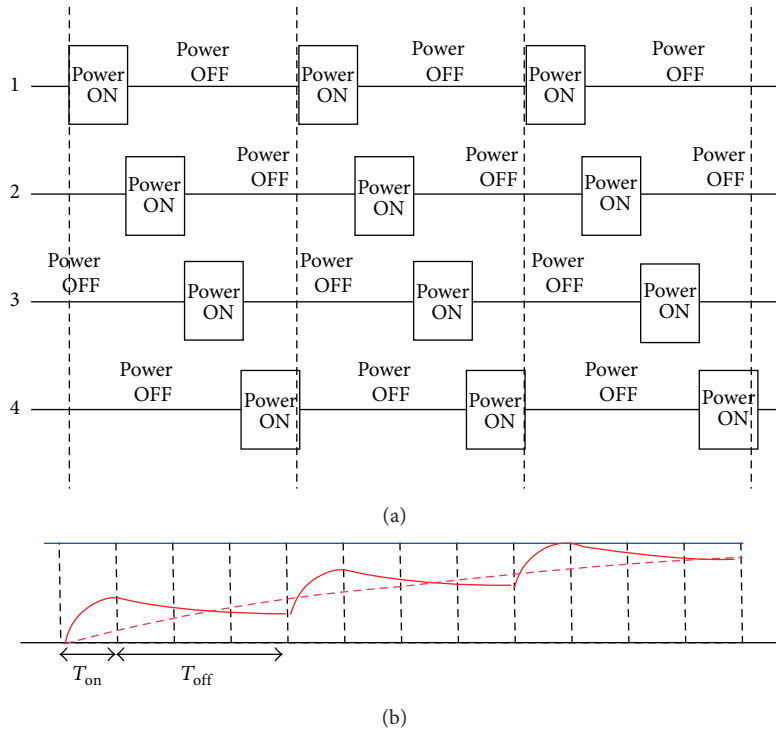


FIGURE 5: Switching applicator operation. Applicator driving time sequence (a) and temperature versus time evolution on the first applicator (b).

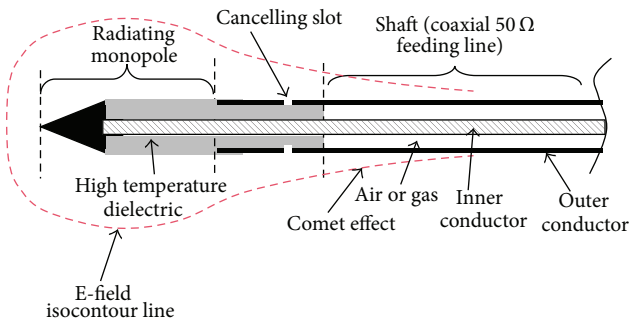


FIGURE 6: The coaxial low loss applicator structure.



FIGURE 7: The coaxial low loss applicator design.

treatment, the shaft can be coated with a very thin layer of Teflon or Parylene C.

High power efficiency is achieved by employing air or gas as dielectric in the coaxial shaft structure and by silver-plating the inner conductor. The applicator can be employed with and without gas cooling, depending on the applied input power. Table 2 resumes the main performances of the different sized applicators with and without CO₂ internal cooling.

Figure 8 shows the ice crystals formation on the applicator’s shaft surface due to the Joule-Thompson effect when the cryogenic gas cooling is employed [24].

Very thin thermal sensors [25, 26] can be incorporated inside the applicator to monitor the temperature in correspondence with its radiating section and along the shaft.

A short circuited $\lambda/4$ stub integrated in the needle handle (shown in Figure 6) is employed to decouple the input port

TABLE 2: Applicators performances.

Size	11 G	14 G	17 G	18 G
Shaft diameter (mm)	3	2.1	1.52	1.27
Efficiency (20 cm shaft length)	0.99	0.96	0.94	0.92
Max CW power (W) (uncooled)	33	20	13	7
Max CW power (W) (cooled)	65	40	26	20

of the applicator from its fluidic section, thus allowing a matched connection with a 50 Ω coaxial cable that was chosen to have <1.5 dB/m loss and to be enough flexible.



FIGURE 8: Ice crystals on the applicator's shaft surface.

Note that if we take into account the insertion losses of the whole power distribution chain (cables, connectors, and MSU) overall efficiencies practically halve and input powers double.

The applicator has been designed using the CST Microwave Studio Electromagnetic Simulation software (CST—Computer Simulation Technology—<https://www.cst.com/>). An optimization method has been employed in order to guarantee the maintenance of a good input matching ($S_{11} < -15$ dB at 2.45 GHz) during the entire ablative procedure, taking into account the variation of the tissue (liver, kidney, and muscle) complex permittivity with temperature and time [27].

4. System Safety and Risk Management

As other MW and RF thermal ablation equipment, TAMMS represents a great challenge from the safety standpoint. Starting from the conception phase, the first step that has been taken into account is a comprehensive risk analysis and assessment, mainly conducted with International Standard ISO 14971:2012 “*Application of Risk Management to Medical Devices*.” The lack of particular standards regarding the safety and effectiveness of surgical MW equipment forces the risk management process to be based only on the general standard EN 60601-1:2006 “*General Requirements for Basic Safety and Essential Performance*” and its corresponding relevant collateral standards (e.g., EN 60601-1-2:2007 related to EM compatibility and EN 60601-1-8 related to alarm systems).

During the risk management process we used the Failure Mode, Effects and Criticality Analysis (FMECA) mainly because of its flexibility in the definition and calibration of risk parameters (i.e., hazard likelihood, severity, and detectability). Indeed the use of the FMECA framework led to the definition of a multiattribute analysis where all the dimensions of service effectiveness were taken into account. To shape and refine the TAMMS project, an exhaustive study of the MWA process in terms of activities, information flows, tools, and different professional profiles involved has also been executed by means of a workflow analysis according to ANSI Standard ANSI/PMI 99/001/2008.

During each project step, the entire system underwent a thorough usability analysis according to the collateral standard EN 60601-1-6:2010, aimed to ensure a user-friendly and safe design.

Finally, every identified risk, including the additional ones closely related to the mitigation interventions themselves, has been brought back under the acceptability threshold. Therefore, the device is ready to go further towards a clinical evaluation and all the next steps needed for CE marking [28]. The entire system is now subject to an intensive engineering process and it will be renamed as Thermal Ablation Treatments for Oncology (TATO).

5. Conclusions

A 2.45 GHz MWA system has been developed with four output channels that can independently feed up to four high efficiency applicators.

The power distribution among the output channels is made by a state-of-the-art solid-state MSU that operates as an active programmable power splitter by employing an FSS technology.

Due to the thermal inertia of the biological tissue and to the very fast commutation of the switching unit, the new system practically performs as a pseudoasynchronous system as demonstrated by EM and TH numerical simulations and confirmed by *ex vivo* experiments (see Appendices A and B).

The novel approach used for feeding multiple applicators allows

- (i) reducing system complexity and cost because only a single high power MW generator is employed;
- (ii) increasing operational flexibility;
- (iii) obtaining thermal lesions of up to 4 cm in diameter with optimal reproducibility and predictability, by using a couple of 17 G uncooled high efficiency applicators (see Appendix B);
- (iv) reducing sensitivity to the placement of applicators and temperature sensors into the tissue.

Future studies and developments will be devoted to the following topics:

- (i) radiometric temperature sensing during the OFF applicator's states;
- (ii) blood flow estimation by measuring the tissue time constant τ during an ON-OFF cycle;
- (iii) adaptive control of the switching duty-cycle based on the temperature feedback;
- (iv) study of a radically new applicator cooling system based on heat-pipe technology;
- (v) integration with robotic and EM navigation technologies.

Appendices

A. Single and Dual-Probe Numerical Simulations

Numerical EM and TH simulations represent a powerful means to estimate the performances of a single or multiapplicator system operating in a biological tissue with the purpose

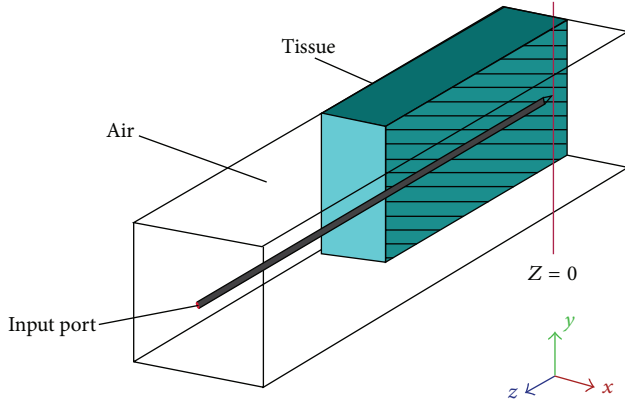


FIGURE 9: CST analysis domain.

TABLE 3: Properties of muscle tissue at 2.45 GHz frequency.

Property at 37°C	Value
Electrical and mechanical properties	
Relative permittivity ϵ_r	45.6
Electrical conductivity σ (S/m)	1.97
Thermal conductivity k_t (W/mK)	0.564
Specific heat c_p (J/kgK)	3400
Density ρ (kg/m ³)	1050
Blood perfusion properties	
Flow coefficient (W/K/m ³)	2700
Metabolic rate (W/m ³)	480

of inducing hyperthermia or producing thermal ablation. In the following we analyze single and double applicator configurations that are the most frequently used in clinical practice, using the CST Microwave Studio software. The analysis domain is shown in Figure 9. Comparisons between synchronous and switched-mode feeding for a couple of applicators are also made.

Steady-state and transient thermal analyses, based on the bioheat equation [29, 30], are performed with the simplifying hypothesis that EM and TH equations are not coupled through the temperature dependence of the tissue permittivity.

The reference tissue chosen for the simulations is muscle, whose properties at 37°C and 2.45 GHz frequency are listed in Table 3.

Figure 10 shows the power density distribution produced by a 17 G applicator with (a) and without (b) cancelling slot. The corresponding steady-state temperature distributions obtained with an effective input power of 15 W and active blood perfusion are depicted in Figure 11.

Note that the “comet tail” clearly evident in the power density distribution practically disappears in the temperature behavior because of the heat sink effect of blood perfusion.

Passing to a couple of 17 G slotted applicators immersed in the same tissue at distance $D = 12$ mm, we obtain the relevant power density distributions depicted in Figure 12. Left figures (a, b, and c) refer to the xy plane ($z = 21$ mm) while right

figures (d, e, and f) refer to yz plane ($x = y = 0$). Upper figures (a, d) represent power densities in the case of in-phase feeding of both applicators, while central (b, e) and lower (c, f) figures represent the two complementary states of a switched feeding.

In both in-phase and switched feeding modalities near field interferences arise in the close proximity of the applicators’ tips. In the first case the interference is “active” and produces focusing in the yz plane of symmetry while in the second case the interference is “passive” and the OFF applicator performs as a wire reflector of the ON applicator. Due to the very high attenuation of the EM fields in the medium the interference phenomena are substantially reduced at a radial distance greater than the plane wave penetration depth in the tissue, that is 20 mm in the muscle at 2.45 GHz. To evidence this phenomenon a reference circle has been traced having radius equal to the penetration depth δ .

Figure 13 refers to simulated treatments of 3 min (a, b) and 10 min (c, d) duration with 40 W total input power.

By increasing the distance D between the two applicators, similar behaviors can be observed up to the $D = 20$ mm limit. Beyond this limit some indentations begin to appear in the 60°C isotherm profile [31].

By increasing the treatment time, the 60°C isotherm that encloses the tissue volume where acute cellular necrosis instantly occurs slightly overtakes the reference circle but does not expand further for $t > 15$ min. This numerical result confirms that treatment times lasting more than 10 minutes are not advantageous at MW frequencies as it happens in RFA. Further simulations proved that the 85% of the maximum allowable size of the thermal lesion is reached only 6 minutes after the treatment starting.

From the totality of the simulations performed we observed that the isotherms for $T \leq 60^\circ\text{C}$ are practically independent from the feeding modality (synchronous, asynchronous, or FSS) because of the heat diffusion inside the tissue.

B. Ex Vivo Experiments

To support numerical analysis’ results, we made single applicator and multiapplicator tests using 14 G devices that were chosen because of their higher power capability with and without a cooling system. The ablations were performed on swine livers or loin pieces taken from animals euthanized less than 6 hours prior to the tests. All tissues were maintained at room temperature. During this work, we will refer to the “input effective power” P_{eff} as the net power flowing in the applicator input port that is calculated by calling off the losses of the power distribution chain. Practically this power value can be obtained by halving the power delivered by the MW generator.

Figure 14 shows ablations obtained employing a single slotted applicator with $P_{\text{eff}} = 15$ W input power and 8-minute treatment time. The thermal lesion was 4×2.5 cm and its shape and dimensions agree well with simulation results.

We have also compared the lesions obtained with and without cooling, shown in Figure 15. With $P_{\text{eff}} = 20$ W and

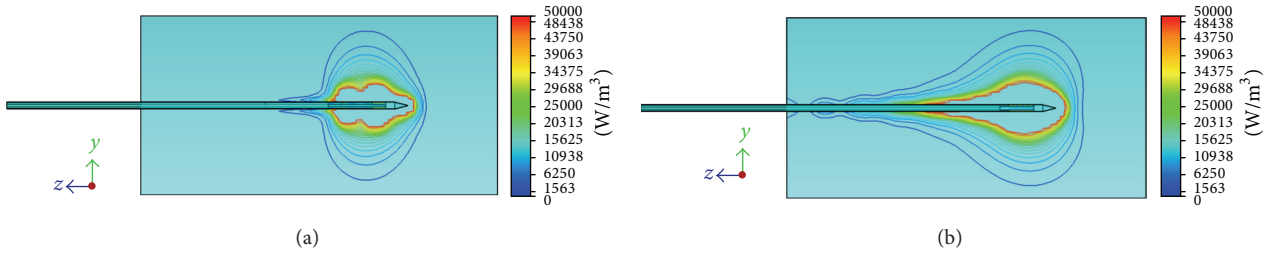


FIGURE 10: Power density distribution on the yz plane of a 17 G applicator operating inside muscle tissue with (a) and without (b) cancelling slot. Reference input power = 1 W.

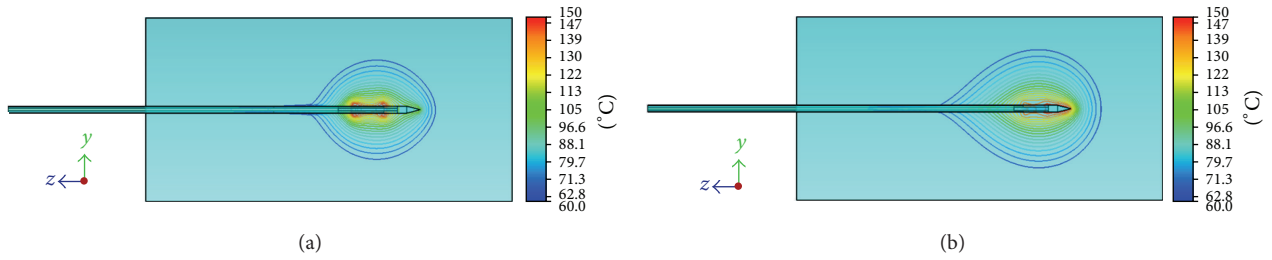


FIGURE 11: Steady-state temperature distribution on the yz plane of a 17 G applicator operating inside muscle tissue with (a) and without (b) cancelling slot. $P_{in} = 15$ W.

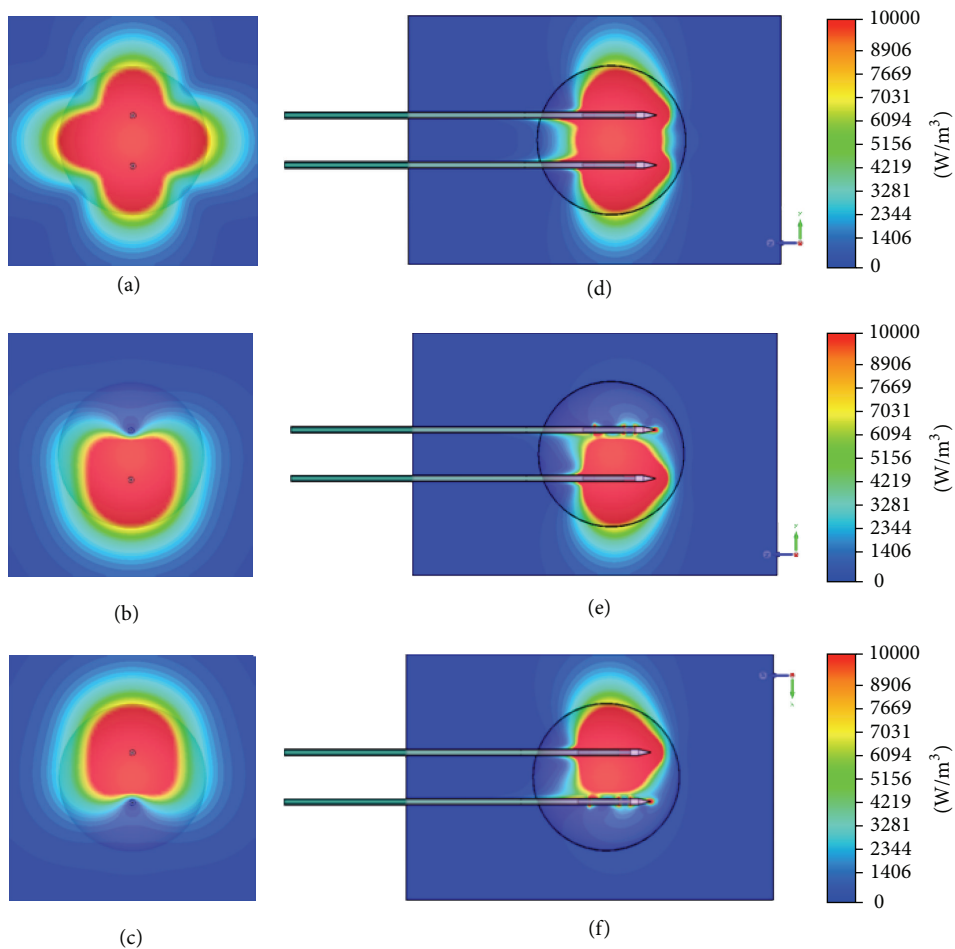


FIGURE 12: Power density distribution produced by a couple of applicators with in-phase feeding (a, d) and switched-mode feeding (b, e) and (c, f). Reference input power = 1 W.

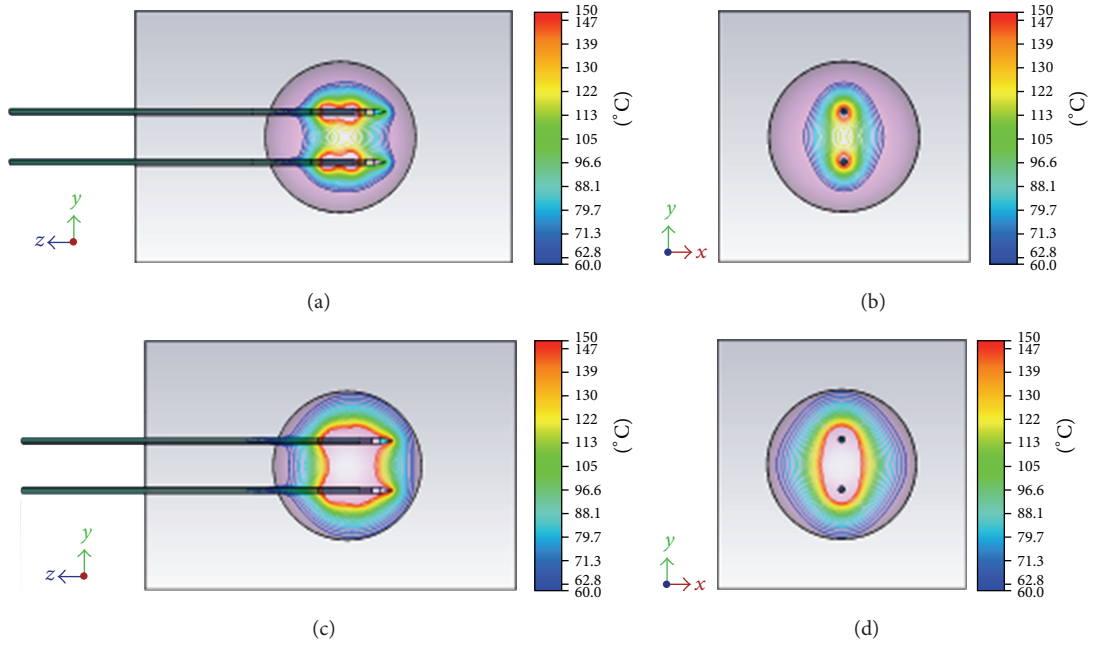


FIGURE 13: Temperature distribution after 3 min (a, b) and 10 min (c, d) simulated treatments in perfused muscle tissue. Total $P_{in} = 40$ W.

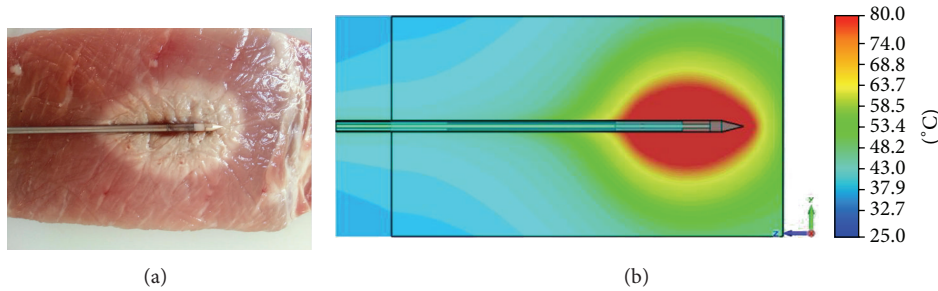


FIGURE 14: Longitudinal cut of the thermal lesion obtained using a single applicator in *ex vivo* swine loin with $P_{eff} = 15$ W (a) and related thermal simulation (b). Treatment time: 8 minutes.

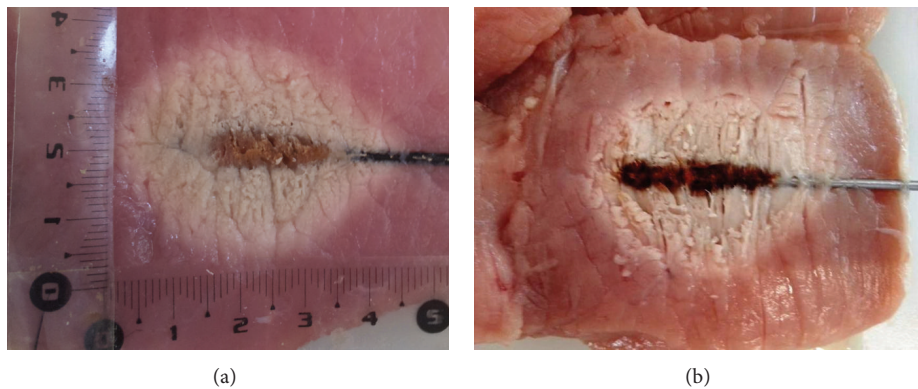


FIGURE 15: Longitudinal cuts of the thermal lesions obtained in *ex vivo* swine loin using a single applicator with $P_{eff} = 20$ W without cooling (a) and $P_{eff} = 30$ W with cooling (b). Treatment time: 10 minutes.

employing an unslotted uncooled applicator, we obtained a lesion of 4.5×3.4 cm with reduced charring in 10 minutes. On the other hand, with cooling active and $P_{eff} = 30$ W, the lesion was 5×4 cm.

From the previous experiments we can observe that the differences between the lesions obtained with and without gas cooling are comparable in shape and dimensions apart from the greater charring produced by the cooled applicator.

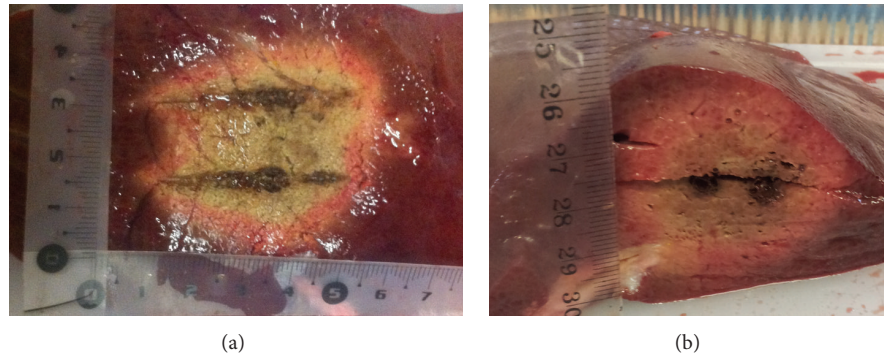


FIGURE 16: Longitudinal (a) and transverse (b) cuts of the thermal lesions obtained in *ex vivo* swine liver using a couple of uncooled applicators with total $P_{\text{eff}} = 40$ W. Treatment time: 10 minutes.

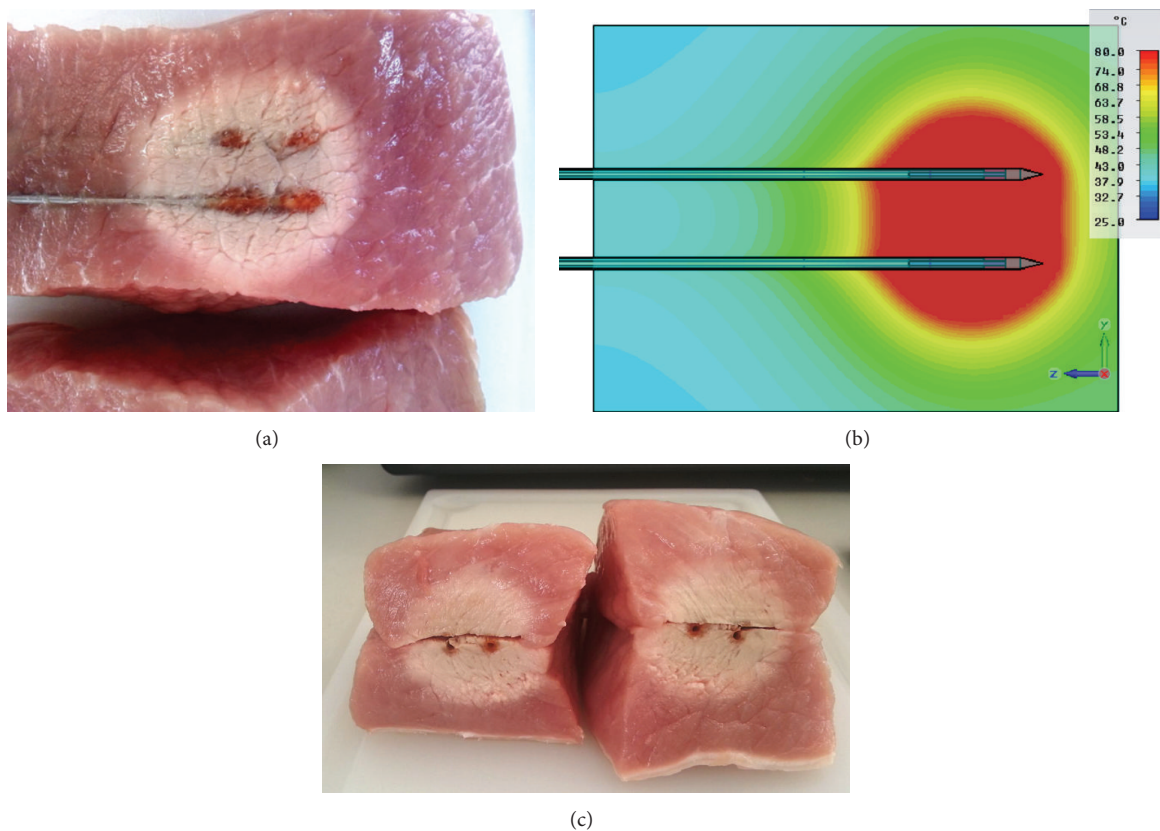


FIGURE 17: Longitudinal cut (a), related thermal simulation (b), and transverse cut (c) of the thermal lesion obtained in *ex vivo* swine loin using a couple of uncooled applicators with total $P_{\text{eff}} = 25$ W. Treatment time: 10 min. One of the two applicators was removed to highlight higher temperature gradient zones.

It follows that, when passing from an uncooled to a cooled device, the efficiency suffers a decrease, about 20% in this case, due to the MW power wasted in the shaft far from the radiating section, where the cooling fluid subtracts heat. This drop of efficiency, that depends on shaft losses and comet effect, is influenced by several parameters such as temperature and flow velocity of the cooling fluid and does not remain constant during the treatment and furthermore cannot easily be measured.

We can ascribe the worse repeatability of the obtained results when the applicator's cooling is active to this variability and unpredictability of the total energy administered to the tissue.

For this reason we decided to perform the multiapplicator trials using only uncooled applicators. Figure 16 shows the longitudinal cut of an ablation made with two applicators on an *ex vivo* swine liver with $P_{\text{eff}} = 40$ W and 10-minute treatment time.

Figure 17 compares the ablation obtained using a couple of applicators immersed in swine loin with the corresponding numerical simulations. Also in this case experiments agree well with simulation results. It is worth noting that we obtained an almost spherical lesion with a 4 cm diameter and negligible charring effects, resulting in a volume of 31 cm³. This finding confirms the preliminary results obtained in [18] using applicators without cap loading.

Referring to recent comparisons [31, 32], it can be said that the ablations shown in Figures 14–17 represent very promising findings, even when compared to the results obtainable with other commercially available systems using cooled applicators.

Abbreviations

CW:	Continuous wave
EM:	Electromagnetic
FIT:	Finite integration technique
FMECA:	Failure Mode, Effects and Criticality Analysis
FSS:	Fast sequential switching
HMI:	Human-machine interface
HPA:	High power amplifier
MPA:	Microwave power amplifier
MSU:	Microwave switching unit
MW:	Microwave
MWA:	Microwave ablation
PAE:	Power added efficiency
PML:	Perfect matched layer
RFA:	Radiofrequency ablation
SBC:	Single board computer
SP4T:	Single pole 4 throw
TH:	Thermal
TAMMS:	Thermal ablation multiprobe microwave system
TATO:	Thermal Ablation Treatments for Oncology.

Conflict of Interests

The authors declare that there is no conflict of interests regarding the publication of this paper.

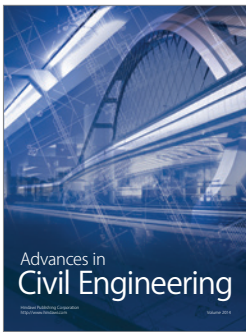
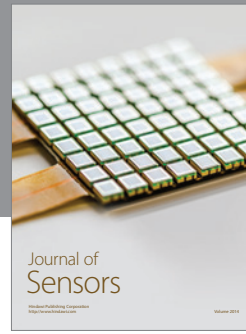
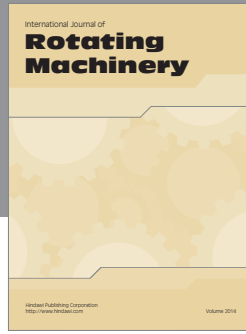
Acknowledgments

The authors would like to gratefully thank the COMIS (Centro Interdipartimentale Sviluppo di Nuove Tecnologie Mini-Invasive in Chirurgia Oncologica) for the highly skilled support in the *ex vivo* experiments. They would like to inform the reader that at the time when they originally wrote the paper, Engineer Vasco Tesi, Ph.D., and Engineer Cosimo Ignesti, they worked at the University of Florence as researchers along with Professor Biffi Gentili. At the present time they collaborate with Wavecomm and Biomedical, respectively, to continue the project and its related studies.

References

- [1] C. Toso, G. Mentha, N. M. Kneteman, and P. Majno, "The place of downstaging for hepatocellular carcinoma," *Journal of Hepatology*, vol. 52, no. 6, pp. 930–936, 2010.
- [2] F. J. Wolf, D. J. Grand, J. T. Machan, T. A. DiPetrillo, W. W. Mayo-Smith, and D. E. Dupuy, "Microwave ablation of lung malignancies: effectiveness, CT findings, and safety in 50 patients," *Radiology*, vol. 247, no. 3, pp. 871–879, 2008.
- [3] C. J. Diederich, "Thermal ablation and high-temperature thermal therapy: overview of technology and clinical implementation," *International Journal of Hyperthermia*, vol. 21, no. 8, pp. 745–753, 2005.
- [4] L. Boni, A. Benevento, F. Cantore, G. Dionigi, F. Rovera, and R. Dionigi, "Technological advances in minimally invasive surgery," *Expert Review of Medical Devices*, vol. 3, no. 2, pp. 147–153, 2006.
- [5] P. Liang, Y. Wang, X. Yu, and B. Dong, "Malignant liver tumors: treatment with percutaneous microwave ablation—complications among cohort of 1136 patients," *Radiology*, vol. 251, no. 3, pp. 933–940, 2009.
- [6] C. L. Brace, "Microwave tissue ablation: biophysics, technology, and applications," *Critical Reviews in Biomedical Engineering*, vol. 38, no. 1, pp. 65–78, 2010.
- [7] T. P. Ryan, P. F. Turner, and B. Hamilton, "Interstitial microwave transition from hyperthermia to ablation: historical perspectives and current trends in thermal therapy," *International Journal of Hyperthermia*, vol. 26, no. 5, pp. 415–433, 2010.
- [8] C. L. Brace, "Radiofrequency and microwave ablation of the liver, lung, kidney, and bone: what are the differences?" *Current Problems in Diagnostic Radiology*, vol. 38, no. 3, pp. 135–143, 2009.
- [9] C. L. Brace, "Microwave ablation technology: what every user should know," *Current Problems in Diagnostic Radiology*, vol. 38, no. 2, pp. 61–67, 2009.
- [10] M. G. Lubner, C. L. Brace, J. L. Hinshaw, and F. T. Lee Jr., "Microwave tumor ablation: mechanism of action, clinical results, and devices," *Journal of Vascular and Interventional Radiology*, vol. 21, no. 8, pp. S192–S203, 2010.
- [11] C. L. Brace, P. F. Laeseke, L. A. Sampson, T. M. Frey, D. W. Van Der Weide, and F. T. Lee Jr., "Microwave ablation with multiple simultaneously powered small-gauge triaxial antennas: results from an in vivo swine liver model," *Radiology*, vol. 244, no. 1, pp. 151–156, 2007.
- [12] M. G. Lubner, J. L. Hinshaw, A. Andreano, L. Sampson, F. T. Lee Jr., and C. L. Brace, "High-powered microwave ablation with a small-gauge, gas-cooled antenna: initial ex vivo and in vivo results," *Journal of Vascular and Interventional Radiology*, vol. 23, no. 3, pp. 405–411, 2012.
- [13] P. Laeseke, F. Lee, D. van der Weide, and C. Brace, "Multiple-antenna microwave ablation: spatially distributing power improves thermal profiles and reduces invasiveness," *Journal of Interventional Oncology*, vol. 5, no. 5, pp. 65–72, 2009.
- [14] A. S. Wright, F. T. Lee Jr., and D. M. Mahvi, "Hepatic microwave ablation with multiple antennae results in synergistically larger zones of coagulation necrosis," *Annals of Surgical Oncology*, vol. 10, no. 3, pp. 275–283, 2003.
- [15] C.-H. Liu, R. S. Arellano, R. N. Uppot, A. E. Samir, D. A. Gervais, and P. R. Mueller, "Radiofrequency ablation of hepatic tumours: Effect of post-ablation margin on local tumour progression," *European Radiology*, vol. 20, no. 4, pp. 877–885, 2010.
- [16] T. Nakazawa, S. Kokubu, A. Shibuya et al., "Radiofrequency ablation of hepatocellular carcinoma: correlation between local tumor progression after ablation and ablative margin," *The American Journal of Roentgenology*, vol. 188, no. 2, pp. 480–488, 2007.

- [17] C. L. Brace, P. F. Laeseke, L. A. Sampson, D. W. van der Weide, and F. T. Lee, "Switched-mode microwave ablation: less dependence on tissue properties leads to more consistent ablations than phased arrays," in *Proceedings of the Radiological Society of North America Meeting (RSNA '07)*, Chicago, Ill, USA, 2007.
- [18] G. Biffi Gentili and M. Linari, "A novel thermo-ablative microwave multi-applicator system," in *Proceedings of the 19th Italian National Meeting on Electromagnetism (RiNEM '12)*, Rome, Italy, September 2012.
- [19] M. F. Iskander and A. M. Tumei, "Design optimization of interstitial antennas," *IEEE Transactions on Biomedical Engineering*, vol. 36, no. 2, pp. 238–246, 1989.
- [20] K. Saito, Y. Hayashi, H. Yoshimura, and K. Ito, "Numerical analysis of thin coaxial antennas for microwave coagulation therapy," in *Proceedings of the IEEE Antennas and Propagation Society International Symposium*, vol. 2, pp. 992–995, Orlando, Fla, USA, July 1999.
- [21] M. Cavagnaro, C. Amabile, P. Bernardi, S. Pisa, and N. Tosoratti, "A minimally invasive antenna for microwave ablation therapies: design, performances, and experimental assessment," *IEEE Transactions on Biomedical Engineering*, vol. 58, no. 4, pp. 949–959, 2011.
- [22] K. Ito, K. Ueno, M. Hyodo, and H. Kasai, "Interstitial applicator composed of coaxial ring slots for microwave hyperthermia," in *Proceedings of the International Conference on Intelligent Systems Applications to Power Systems (ISAP '89)*, pp. 253–256, Tokyo, Japan, 1989.
- [23] I. Longo, G. B. Gentili, M. Cerretelli, and N. Tosoratti, "A coaxial antenna with miniaturized choke for minimally invasive interstitial heating," *IEEE Transactions on Biomedical Engineering*, vol. 50, no. 1, pp. 82–88, 2003.
- [24] E. M. Knavel, J. L. Hinshaw, M. G. Lubner et al., "High-powered gas-cooled microwave ablation: shaft cooling creates an effective stick function without altering the ablation zone," *The American Journal of Roentgenology*, vol. 198, no. 3, pp. W260–W265, 2012.
- [25] M. Linari and G. Biffi Gentili, "Design and optimization of a miniaturized hyperthermic microwave applicator with integrated temperature sensors," in *Proceedings of the 10th International Congress on Hyperthermic Oncology (ICHO '08)*, 2008.
- [26] G. B. Gentili and M. Linari, "A minimally invasive microwave hyperthermic applicator with an integrated temperature sensor," in *Proceedings of the 1st International Conference on Biomedical Electronics and Devices (BIODEVICES '08)*, pp. 113–118, January 2008.
- [27] Z. Ji and C. L. Brace, "Expanded modeling of temperature-dependent dielectric properties for microwave thermal ablation," *Physics in Medicine and Biology*, vol. 56, no. 16, pp. 5249–5264, 2011.
- [28] E. Iadanza, C. Ignesti, and G. B. Gentili, "Risk management process in a microwave thermal ablation system for CE marking," in *XIII Mediterranean Conference on Medical and Biological Engineering and Computing 2013*, vol. 41 of *IFMBE Proceedings*, pp. 1170–1173, 2014.
- [29] H. H. Pennes, "Analysis of tissue and arterial blood temperatures in the resting human forearm," *Journal of Applied Physiology*, vol. 85, no. 1, pp. 5–34, 1998.
- [30] W. L. Nyborg, "Solutions of the bio-heat transfer equation," *Physics in Medicine and Biology*, vol. 33, no. 7, pp. 785–792, 1988.
- [31] F. Oshima, K. Yamakado, A. Nakatsuka, H. Takaki, M. Makita, and K. Takeda, "Simultaneous microwave ablation using multiple antennas in explanted bovine livers: relationship between ablative zone and antenna," *Radiation Medicine—Medical Imaging and Radiation Oncology*, vol. 26, no. 7, pp. 408–414, 2008.
- [32] R. Hoffmann, H. Rempp, L. Erhard et al., "Comparison of four microwave ablation devices: an experimental study in ex vivo bovine liver," *Radiology*, vol. 268, no. 1, pp. 89–97, 2013.



Hindawi

Submit your manuscripts at
<http://www.hindawi.com>

